

Research Paper

Development of an Accurate and Proactive Immunomodulatory Strategy to Improve Bone Substitute Material-Mediated Osteogenesis and Angiogenesis

Zhi-wei Zheng^{1,2*}, Ya-hong Chen^{3*}, Ding-yu Wu^{4*}, Jin-bing Wang^{1,2}, Ming-ming Lv^{1,2}, Xian-song Wang⁴✉, Jian Sun^{1,2}✉, Zhi-Yong Zhang^{5,6}✉

1. Department of Oral and Maxillofacial-Head and Neck Oncology, Shanghai Ninth People's Hospital, Shanghai Jiao Tong University School of Medicine, Shanghai, 200011, China.
2. Shanghai Key Laboratory of Stomatology & Shanghai Research Institute of Stomatology; National Clinical Research Center of Stomatology, Shanghai Ninth People's Hospital, Shanghai Jiao Tong University School of Medicine, Shanghai, 200011, China.
3. Department of Plastic and Reconstructive Surgery, Shanghai Ninth People's Hospital, Shanghai Jiao Tong University School of Medicine, Shanghai, 200011, China.
4. Shanghai Key Laboratory of Tissue Engineering, Shanghai Ninth People's Hospital, Shanghai Jiao Tong University School of Medicine, Shanghai, 200011, China.
5. Translational Research Centre of Regenerative Medicine and 3D Printing Technologies of Guangzhou Medical University, The Third Affiliated Hospital of Guangzhou Medical University, Guangzhou, Guangdong 510150, China.
6. China Orthopedic Regenerative Medicine Group (CORMed), Hangzhou, 310058, China.

*Authors have equally contributed to the work in this study.

✉ Corresponding authors: E-mail address: mr.zhiyong@gmail.com (Z.-Y. Zhang), jianjian60@yahoo.com (J. Sun), wonderluis@126.com (X. W).

© Ivyspring International Publisher. This is an open access article distributed under the terms of the Creative Commons Attribution (CC BY-NC) license (<https://creativecommons.org/licenses/by-nc/4.0/>). See <http://ivyspring.com/terms> for full terms and conditions.

Received: 2018.07.05; Accepted: 2018.10.04; Published: 2018.10.29

Abstract

Background: Treatment of large bone defects represents a major clinical problem worldwide. Suitable bone substitute materials are commonly required to achieve successful bone regeneration, and much effort has been spent to optimize their chemical compositions, 3D architecture and mechanical properties. However, material-immune system interactions are increasingly being recognized as a crucial factor influencing regeneration. Here, we envisioned an accurate and proactive immunomodulation strategy via delivery of IL-4 (key regulator of macrophage polarization) to promote bone substitute material-mediated regeneration.

Methods: Four different IL-4 doses (0 ng, 10 ng, 50 ng and 100 ng) were delivered into rat large cranial bone defects at day 3 post-operation of decellularized bone matrix (DBM) material implantation, and the osteogenesis, angiogenesis and macrophage polarization were meticulously evaluated.

Results: Micro-CT analysis showed that immunomodulation with 10 ng IL-4 significantly outperformed the other groups in terms of new bone formation (1.23-5.05 fold) and vascularization (1.29-6.08 fold), achieving successful defect bridging and good vascularization at 12 weeks. Histological analysis at 7 and 14 days showed that the 10 ng group generated the most preferable M1/M2 macrophage polarization profile, resulting in a pro-healing microenvironment with more IL-10 and less TNF- α secretion, a reduced apoptosis level in tissues around the materials, and enhanced mesenchymal stem cell migration and osteogenic differentiation. Moreover, *in vitro* studies revealed that M1 macrophages facilitated mesenchymal stem cell migration, while M2 macrophages significantly increased cell survival, proliferation and osteogenic differentiation, explaining the *in vivo* findings.

Conclusions: Accurate immunomodulation via IL4 delivery significantly enhanced DBM-mediated osteogenesis and angiogenesis via the coordinated involvement of M1 and M2 macrophages, revealing the promise of this accurate and proactive immunomodulatory strategy for developing new bone substitute materials.

Key words: bone substitutes, immunomodulation, osteogenesis, angiogenesis, macrophages

Introduction

Bone defects caused by trauma and disease represent a major clinical problem worldwide. Large bone defects fail to heal spontaneously and require implantation of biomaterial-based bone substitutes to achieve bone tissue regeneration [1]. Over the last several decades, numerous experiments have been performed to fabricate an ideal bone substitute material [2, 3]. Typical screening of such material involves *in vitro* and *in vivo* experiments to investigate biomaterial attributes, including biocompatibility and bioactivity. In addition, many strategies have been developed to optimize the material composition, 3D architecture and mechanical properties to improve its biological performance [1,4-6]. However, more recently, increasing evidence has demonstrated that the host immune reaction following implantation of bone substitute material determines the success of bone regeneration [7, 8].

Inflammation is recognized as a crucial component of *in vivo* bone injury repair that influences the outcome [9]. The processes of bone repair are biologically associated with those of the host immune response, sharing a number of cytokines, receptors and signaling molecules [1, 7]. Accordingly, in recent studies, the host immune response against bone substitute material has been increasingly explored [8, 10-16]. These studies have primarily focused on changes in material properties affecting immune cells, such as surface topography [11], porosity [15] and release ions [8, 13]. However, material properties are not able to accurately modulate the material-host response due to its complex biological nature, and most of these studies have been performed as retrospective and passive observations of immune cell phenotypes associated with successful biomaterials [8, 16]. Consequently, recent studies have begun to evaluate improvements in regenerative outcomes after immunomodulation by cytokines delivered from the material [17-19]. However, the immunomodulation is a 'double-edged sword', and different extents of immunomodulation lead down different paths. Research that accurately and proactively modulates the material-host response is required to further optimize the immunomodulatory strategy and may hold great promise in the context of advanced bone substitute material design.

Here, we envisioned a new strategy to accurately and proactively modulate the host immune response via cytokine delivery to improve bone substitute material-mediated osteogenesis and angiogenesis. Recently, macrophage-material interactions have received particular attention because macrophages

are the central cell type in directing host inflammatory and immune processes. A spectrum of macrophage phenotypes contained between two extremes have been identified, ranging from pro-inflammatory (M1) to anti-inflammatory (M2) phenotypes, with significant implications in disease [20], wound healing [21, 22] and biomaterial performance [18]. The findings of studies in nearly all organ systems have demonstrated that re-establishment of the normal homeostatic state after wounding is often associated with the M2 macrophage profile [18, 19, 21].

In the present study, we accurately and proactively construct and optimize the inflammatory microenvironment via the classic M2-polarizing cytokine (IL-4) [23] and evaluate its potential in promoting material-mediated osteogenesis and the related angiogenesis. A decellularized bone matrix (DBM) material commonly utilized in bone repair was chosen as a model bone substitute material. First, post-operation of DBM material implantation into rat large cranial bone defects, four different IL-4 doses (0 ng, 10 ng, 50 ng and 100 ng) were delivered into the defect region, and the results demonstrated that accurate and proactive immunomodulation via 10 ng of IL-4 promoted neo-vascularization of the DBM and achieved nearly complete healing of the cranial defect at 12 weeks. Next, the M1/M2 macrophage polarization and local inflammatory microenvironment were evaluated. Finally, the potential effects of polarized macrophages on bone mesenchymal stem cell (BMSC) migration, survival, proliferation and osteogenic differentiation were examined.

Methods

***In vivo* Defect Studies: Large cranial bone defect model**

To explore the effects of the accurate and proactive immunomodulatory strategy on material-mediated osteogenesis and angiogenesis, a rat large cranial bone defect model was constructed as previously described [24, 25]. DBM scaffolds prepared from porcine caput femoris as previously described [26, 27], were selected as the model material. Scaffolds (5 mm diameter and 1.5 mm in height) were separated based on dry weight, sterilized in 70% ethanol, rinsed and incubated in PBS before implantation. The biocompatibility of the DBM was evaluated via imaging of BMSCs seeded on the scaffolds after 7 days using scanning electron microscopy (SEM) (Figure 1A).

The study protocol was approved by the Ethics Committee of Shanghai Ninth People's Hospital Affiliated Shanghai Jiao Tong University School of

Medicine and followed the National Institutes of Health Guide concerning the Care and Use of Laboratory Animals. Only 8-week-old male Sprague Dawley rats (180-200 g weight) were selected to avoid the known variables (estrogen and age) affecting bone formation. Briefly, rats were anesthetized via intraperitoneal pentobarbital injection. Then, a 2.0-cm sagittal incision was made in the middle of the scalp to expose the calvarium. The periosteum was deflected using a periosteal elevator, and a 5-mm size defect in the center region on each rat calvaria was created using a trephine that was constantly cooled with sterile saline. The dura mater was kept intact, as in craniostomy surgeries [28, 29]. After a thorough rinse with saline, the scaffold was implanted within the defect.

At day 3 post-operation, the animals were anesthetized, and 10, 50 or 100 ng IL-4 resuspended in 20 μ L saline was injected through the skin directly over the scaffolds. The needle was kept in place for 30 s after the injection and then removed slowly. The same volume of vehicle alone was used as the control (0 ng). Daily injection of IL-4 was performed from day 3 to day 7. A schematic illustration of the process is shown in Figure 1A.

Histological observation of the short-term inflammatory microenvironment

For examination of the dynamic infiltration of inflammatory cells, 8 rats from each group were sacrificed at 7 and 14 days post-surgery, and the scaffold and surrounding tissues were collected for subsequent histopathology and immunohistochemistry.

Immunohistochemistry and immunofluorescence

Completely demineralized specimens were embedded in paraffin to prepare 5- μ m-thick sections for immunohistochemistry. The sections were blocked with 5% bovine serum albumin (Millipore Sigma, St. Louis, MO, USA) and incubated with the following primary antibodies: anti-IL-10, anti-SSEA-4, anti-Runt-related transcription factor 2, anti-osteocalcin (OCN) (Abcam), anti-TNF- α (Affinity Biosciences, OH, USA) and anti-cleaved-Caspase 3 (Cell Signaling Technology, Danvers, MA, USA). The sections were then incubated with peroxidase-conjugated secondary antibody, visualized with 3,3'-diaminobenzidine solution and counterstained with hematoxylin. Digitized images obtained from the stained sections ($n = 6$) were analyzed using Image-Pro Plus software (Media Cybernetics, Inc., Rockville, MD, USA).

For immunofluorescence examination, the

samples were embedded in OCT and frozen. Samples were sectioned into 6- μ m slices and mounted onto slides for histological evaluation. Primary antibodies targeting CD68, CD206 and inducible nitric oxide synthase (iNOS) from Abcam (Cambridge, MA, USA) were used to assess the number, location and phenotypic profiles of macrophages. Secondary antibodies conjugated with fluorescent dyes (Jackson Immuno Research Laboratories, Inc.) were applied under light protection. The nuclei were counterstained with DAPI, and the stained sections were examined using confocal laser scanning microscopy.

Terminal deoxynucleotidyl transferase 2'-deoxyuridine 5'-triphosphate nick end labeling (TUNEL) assay

For detection of apoptosis in the tissue surrounding the material, the sections were routinely deparaffinized and rehydrated. Proteinase K (20 μ g/mL, diluted in Tris/HCl, pH = 7.4) was used for tissue repair at room temperature for 30 minutes. Sections were washed with PBS and incubated with TUNEL reaction mixture (Roche, German). Finally, the sections were washed with PBS and assessed using a fluorescence microscope.

Evaluation of long-term osteogenesis and angiogenesis

At 6 and 12 weeks post-operation, the animals were euthanized, and the rat skulls were harvested and fixed in 4% PFA for osteogenesis and angiogenesis evaluation.

Micro-CT scanning and analysis

The samples were first assessed with a micro-CT scanner (μ CT-80, Scanco Medical, Switzerland) in high-resolution scanning mode [24]. After the micro-CT scans, bone visualization was performed using 3D isosurface renderings. Micro-CT was used to determine the percentage of new bone volume relative to tissue volume (BV/TV) and the bone mineral density (BMD). To analyze vascularization of the defects, Microfil perfusion was used ($n = 3$ each group) at 12 weeks as previously described [25]. Briefly, the samples were extracted and nondecalcified skulls were first measured to identify cranial defects. After 4 weeks of decalcification in 10% EDTA, the samples were scanned by micro-CT again, and 3D images of blood vessels were reconstructed by setting the threshold at 140. Based on these results, the region of interest was identified, and analyses of vascular volume, connectivity and thickness were performed using the micro-CT software.

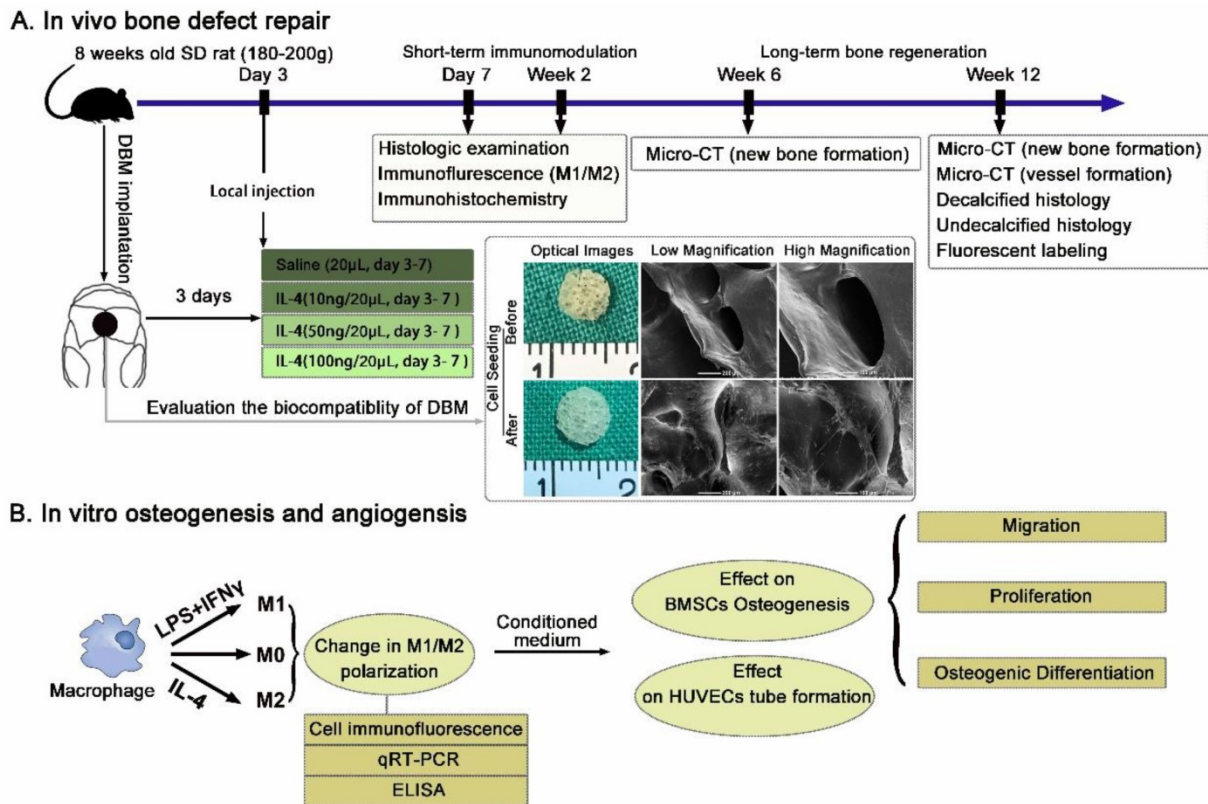


Figure 1. Schematic diagrams of the experimental design and protocol. (A) Experimental design of the *in vivo* evaluation of the accurate and proactive immunomodulatory strategy for material-based rat cranial bone defect repair. DBM material was characterized by SEM imaging and demonstrated outstanding cellular adhesion of BMSCs to scaffolds. (B) The angiogenic and osteogenic effects of macrophage phenotypes were assessed indirectly by co-culturing BMSCs and HUVECs with conditioned media from polarized macrophages.

Double fluorescence labeling and Van Gieson staining

To further evaluate the rate of new bone formation, 4 rats from each group were injected with alizarin red (30 mg/kg; Millipore Sigma) and calcein (20 mg/kg; Millipore Sigma) at 6 and 9 weeks, respectively. The calvarias were harvested at 12 weeks, fixed in 10% formalin overnight, embedded in methyl methacrylate and sectioned through the sagittal plane to produce 50-µm-thick undecalcified sections. Unstained sections were examined using a fluorescence microscope. For each sample, images were acquired randomly (n = 6) for integrated optical density determination of alizarin red and calcein distribution.

After examination for double fluorescence labeling, the sections were then stained with Van Gieson stain to further quantify collagen formation in the defect region. Red particles (indicating collagen fibers) were considered positive. Digitized images obtained from the stained sections (n = 6) were randomly chosen and analyzed using Image-Pro Plus software.

Effects of macrophage phenotype on *in vitro* osteogenesis and angiogenesis

Cell culture

Rat BMSCs were isolated and cultured based on protocols from previous studies [27, 30]. The murine-derived macrophage cell line RAW 264.7 (RAW) was used in this study. RAW cell cultures were maintained in Dulbecco's modified Eagle's medium (DMEM, HyClone) supplemented with 10% heat-inactivated fetal bovine serum (FBS, Gibco) at 37°C in a humidified CO₂ incubator. The growing cells were passaged at approximately 80% confluence by gentle scraping.

Preparation of polarized macrophages and conditioned media

For induction of polarized macrophages, RAW cells were cultured in complete medium with the following cytokines: 100 ng/mL interferon-gamma (IFN γ , Peprotech, Rocky Hill, NJ, USA) and 100 ng/mL lipopolysaccharide (LPS, Sigma) for M1 induction for 24 h. The acquired M1 macrophages were then further treated with 40 ng/mL IL-4 (Peprotech) for 24 h to mimic the biological transition

from M1 to M2 polarization. A small sample was obtained via gentle scraping for phenotype confirmation, and the remaining cells were cultured in serum-free DMEM after two washes with PBS. After 24 h of serum starvation, the conditioned medium was filter sterilized and frozen at -80°C until analysis or use (Figure 1B).

To ensure that certain subtypes were present, immunofluorescence staining with anti-CD206 and anti-iNOS antibodies (Abcam) and DAPI (Life Technology, Carlsbad, CA, USA) was performed. Furthermore, total RNA was harvested using TRIzol reagent to determine polarization-related gene expression (Table S1). The concentrations of inflammatory factors in the conditioned mediums ($n = 4$ each group) were examined with mouse TNF- α and IL-10 Quantikine ELISA kits (ExCellBio, Shanghai, China) according to the manufacturer's instructions.

Effects of conditioned media from RAW cells on *in vitro* chemotaxis stimulation of BMSCs

BMSCs were placed in the upper chamber of Transwell® inserts. Different culture media were placed in the lower chamber according to the following group designation: Control [Ctrl]-DMEM; M0, M1 and M2 group-DMEM previously conditioned with M0, M1 and M2 macrophages, respectively. The migrated cells were stained with DAPI and counted after 6 and 12 h. Experiments were conducted in sextuplicate.

Western blotting

To examine the major factors involved in chemotaxis stimulation, the protein levels of stromal cell-derived factor-1 (SDF-1) and VEGF in polarized macrophages were measured using western blot analysis. Briefly, protein (50 μg) from each specimen was loaded onto a 15% polyacrylamide gel-plate, and the proteins were transferred to a polyvinylidene difluoride membrane (Millipore Sigma) after electrophoresis. The membrane was blocked with 5% nonfat milk and incubated with anti-SDF-1 α (Cell Signaling Technology) and anti-VEGF α antibodies (Abcam) overnight. After incubation with a chemiluminescence reagent (Thermo, USA), visualization of the protein bands was performed via exposure to Kodak X-ray films [25]. Positive immunoreactive bands were quantified densitometrically, and the results were normalized to GAPDH expression.

Effects of conditioned media from RAW cells on *in vitro* cell apoptosis and proliferation

Cells were stained using an apoptosis detection kit (Thermo Scientific, Waltham, MA, USA) according

to the manufacturer's instructions [31]. Briefly, BMSCs were harvested after cultured with different conditioned media or culture medium (Ctrl) supplemented with 10% FBS for 3 days. The BMSCs were then resuspended in $1\times$ annexin-binding buffer (100 μL) and incubated with 1 μL propidium iodide (PI, 100 $\mu\text{g}/\text{mL}$) and 5 μL Annexin V for 30 min in the dark and analyzed via flow cytometry.

Cell proliferation was monitored using Cell Counting Kit-8 (CCK-8) ($n = 6$). Briefly, BMSCs were seeded in 96-well plates at a density of 3×10^3 cells/well and cultured in conditioned media or control medium supplemented with 10% FBS for 1, 3, 5 and 7 days.

Effects of conditioned media from RAW cells on *in vitro* osteogenic differentiation

BMSCs were plated at a density of 5×10^3 cells/ cm^2 . After 24 h of incubation, the culture medium was removed and replaced by conditioned or control medium with osteogenic supplements [10 mM β -glycerophosphate, 50 μM L-ascorbic acid 2-phosphate, 100 nM dexamethasone]. At day 7 after osteogenic induction, the cells were fixed for alkaline phosphatase (ALP) staining and subsequent imaging evaluation using an HP Scanjet G3110 Photo Scanner. ALP activity after 7 and 14 days of culture was quantified using a QuantiChrom™ Alkaline Phosphatase Assay Kit (BioAssay Systems, CA, USA), and the total protein content was assessed with a BCA Protein Assay Kit (Thermo Scientific). At day 14 after osteogenic induction, cells were fixed for Alizarin Red (AR) and DAPI staining and immunofluorescence staining with anti-OCN and anti-Runx-2 antibodies.

Total RNA was harvested after 7 and 14 days of culture to determine osteogenesis-related genes expression [ALP, collagen I (COL1), osteopontin (OPN), RUNX2, bone morphogenetic protein-2 (BMP-2) and OCN].

In vitro sprout formation analysis

Tube formation of human umbilical vein endothelial cells (HUVECs) was monitored as previously reported [32]. Briefly, 25 000 cells were added to each well containing 1 mL of conditioned mediums from (a) M0, (b) M1 and (c) M2 macrophages, with DMEM as the control. After incubation for 12 h in 24-well plates coated with Matrigel growth factor-reduced matrix solution (BD Biosciences, NJ, USA), images were captured under a microscope (Leica). The tubule length and number of segments and nodes in 6 randomly chosen fields were quantified as previously described using the Angiogenesis Analyzer macro in ImageJ [21].

Statistical analysis

The data are presented as the mean \pm SEM. Statistical analysis was performed in GraphPad Prism 5.0 software using one-way ANOVA with post hoc Tukey multiple comparison tests to examine the effects of various IL-4 doses on the parameters investigated. The mean of each column with the mean of every other column were compared. $p < 0.05$ was considered significant.

Results

Evaluation of *in situ* bone and vascular regeneration promoted by accurate and proactive immunomodulation via IL-4

We used a cranial bone defect model to explore the potential of an accurate and proactive immunomodulatory strategy in advanced bone substitute material design. To confirm a role of the accurate and proactive immunomodulatory strategy in improving bone substitute material-mediated osteogenesis and angiogenesis, DBM material commonly utilized in bone repair was chosen as a model bone substitute material. IL-4 (10 ng, 50 ng or 100 ng) was administered via local injection post-implantation of DBM, with DBM without IL-4 administration (0 ng) as a control. At 6 and 12 weeks post-operation, the skulls were collected to confirm the angiogenic and osteogenic effects of different extents of immunomodulation using micro-CT. Defects left untreated and without scaffolds are shown in Figure S1. Obviously, the contour of the defect could be easily identified at 12 weeks post-operation, confirming nonhealing of the 5-mm cranial defect within the experiment period. As expected, 6 weeks after DBM implantation (0 ng IL-4), apparent new bone tissue was formed from the margins of the defect. Of note, significant increases in newly formed bone tissue were observed in both the 10 ng and 50 ng groups when compared with the 0 ng group. At 12 weeks after surgery, the defects were completely filled with new bone in the 10 ng group (Figure 2A). This was further confirmed by quantitative analyses, in which the 10 ng group had the highest BV/TV value (1.23-5.05 fold, $p < 0.05$) as well as the highest BMD (1.33-3.79 fold, $p < 0.05$) compared with the other groups (Figure 2B-C). Conversely, the 100 ng group exhibited the least newly formed bone tissue, and bone-like tissues sporadically crept from the ends of the bone defects.

Angiography was performed at 12 weeks after surgery to evaluate the extent of angiogenesis. The vascular network and connections were more readily identified in the 10 ng and 50 ng groups, and these values were significantly increased in the 10 ng group

compared with the 50 ng group (Figure 2D). The 10 ng group exhibited increased vascular volume (1.29-6.08 fold), connectivity (1.46-7.17 fold) and vascular thickness (1.3-3.42 fold) compared with the other groups ($p < 0.05$) (Figure 2E-G).

Histological assessment of new bone regeneration patterns

H&E and Masson's trichrome staining were used to further evaluate the bone regeneration patterns within the DBM scaffolds at week 12 (Figure 3A, B). Different bone tissue regeneration patterns were observed after administration of different doses of IL-4. The 0 ng group showed a bone tissue in-growth pattern from the peripheral region, while the 10 ng and 50 ng groups displayed a bone tissue in-growth pattern from the peripheral region and an *in situ* bone island formation pattern in the central region. In the 10 ng group, the majority of the defect region was filled with new bone that was integrated with the scaffolds, and consisted of both immature and mature bone, as noted with Masson's trichrome staining. In contrast, in the 100 ng group, the defects were filled with loose connective fibrous tissues surrounding the minimal newly formed bone.

Double fluorescence labeling showed similar results (Figure 3C). The integrated optical density of areas labeled with calcein and alizarin red was observed in the following order: 10 ng group > 50 ng group > 0 ng group > 100 ng group ($p < 0.05$) (Figure 3D). In addition, enhanced bone regeneration in the 10 ng group was observed with Van Gieson staining (Figure 3E). The 10 ng ($31.67 \pm 2.65\%$) and 50 ng ($22.33 \pm 1.52\%$) groups exhibited larger new bone area with better osteointegration compared with the 0 ng ($10.9 \pm 1.1\%$) and 100 ng ($7.2 \pm 0.72\%$) groups (Figure 3F).

Study of the early-stage host response and macrophage polarization with different IL-4 doses

THE DBM and surrounding tissues at days 7 and 14 post-implantation were then harvested to study the local inflammatory responses and macrophage polarization. The histologic appearance of tissue from rats implanted with the DBM was characteristic of a transient inflammatory response, including significant inflammatory cell infiltration at 7 days. Although the cell density appeared higher in the 0 ng group, this reaction was largely resolved within 14 days in all the groups, regardless of IL-4 addition (Figure 4A).

Immunolabeling of CD68 (pan macrophage marker), iNOS (an M1 marker) and CD206 (an M2 marker) was performed to further identify the number, location and phenotypic profiles of

macrophages around the scaffolds. The results revealed marked differences in the macrophage responses at day 7 and 14 post-implantation after the administration of different IL-4 doses. DBM scaffolds without IL-4 were found to be relatively “inert”, and the M2 (CD68⁺ CD206⁺) macrophages stayed at similar level from 7 days to 14 days. As expected, local administration of IL-4 effectively polarized the macrophages toward the M2 phenotype in a dose-dependent manner. Increased numbers of M2 macrophages were noted in the IL-4-treated groups compared with the controls at 7 and 14 days after

surgery (Figure 4B-C). Furthermore, the analysis of M1(CD68⁺ iNOS⁺) macrophages revealed an overall reduction from day 7 to day 14 in all groups, indicating the good biocompatibility of the DBM. However, with the addition of IL-4, a reduction in the M1 macrophage number was observed in the 10 ng and 50 ng groups compared with the 0 ng group. Of note, although M1 macrophage infiltration was reduced in the 100 ng group at 7 days, a prolonged M1 polarization phase was observed at 14 days (Figure 4D-E).

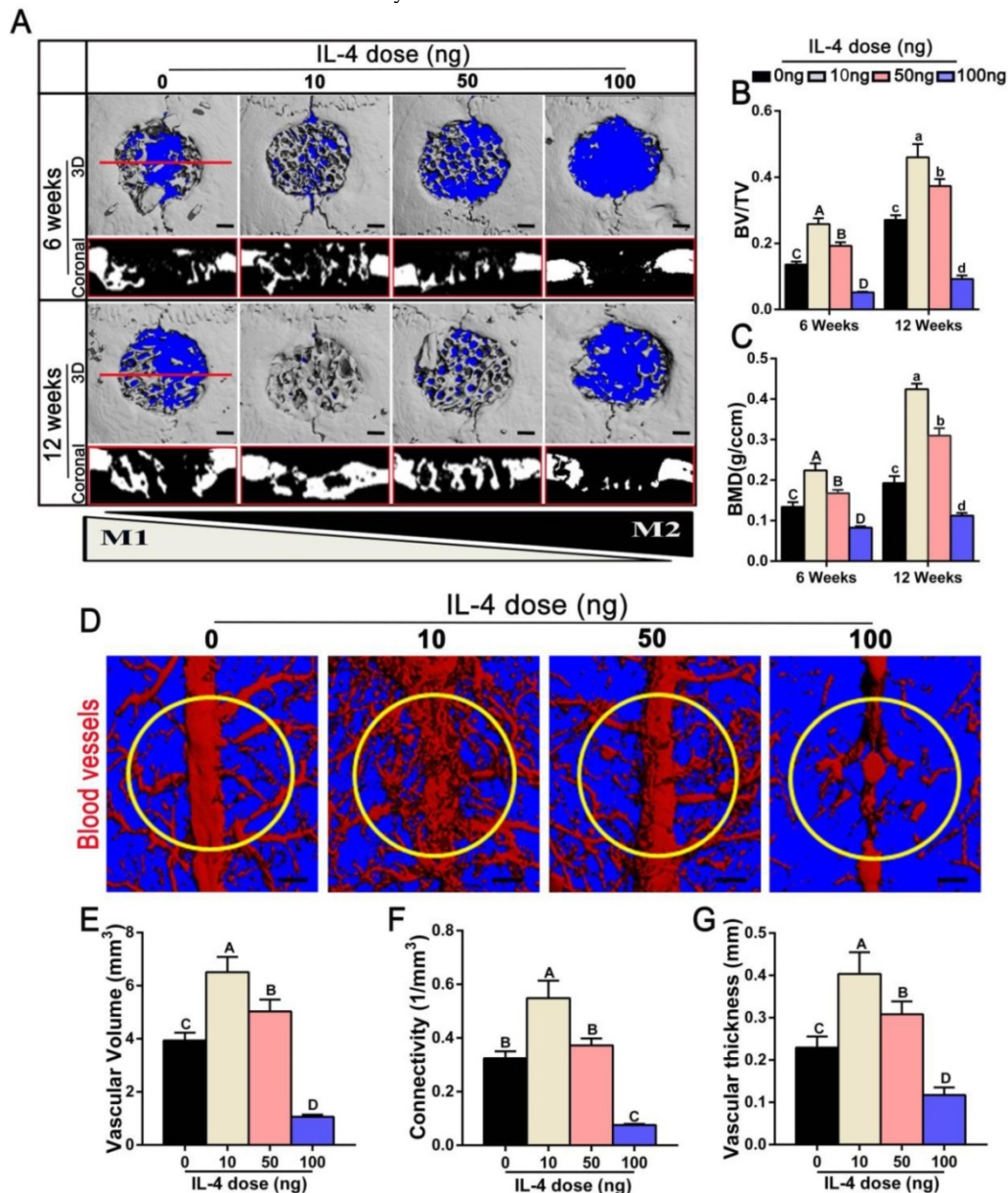


Figure 2. Effects of accurate and proactive immunomodulation via IL-4 on DBM-mediated osteogenesis and angiogenesis in large cranial bone defects. Four doses of IL-4 (0 ng, 10 ng, 50 ng and 100 ng) were used. (A) 3D and coronal micro-CT images of the cranial bone defects at 6 and 12 weeks showing the best defect healing outcome, with complete defect bridging at 12 weeks, in the 10 ng group. This was followed by the 50 ng and 0 ng group, with partial defect bridging; the 100 ng group exhibited non-union healing. Bar = 1 mm. (B) Ratio of bone volume/total volume (BV/TV) and (C) bone mineral density (BMD) showing that the 10 ng group had the highest amount of bone tissue. (D) Micro-CT angiography. The blood vessels were perfused with Microfil. Yellow circles indicate bone defect regions. Bar = 1 mm. (E-G) Summary of micro-CT angiography results. Bar charts showed that the (E) volume of newly-formed vasculature, (F) microvessel connectivity and (G) vascular thickness were greater in the 10 ng group, indicating the most vascular development, compared with the other groups. For all charts, the groups designated by different uppercase letters or lowercase letters were significantly different ($p < 0.05$).

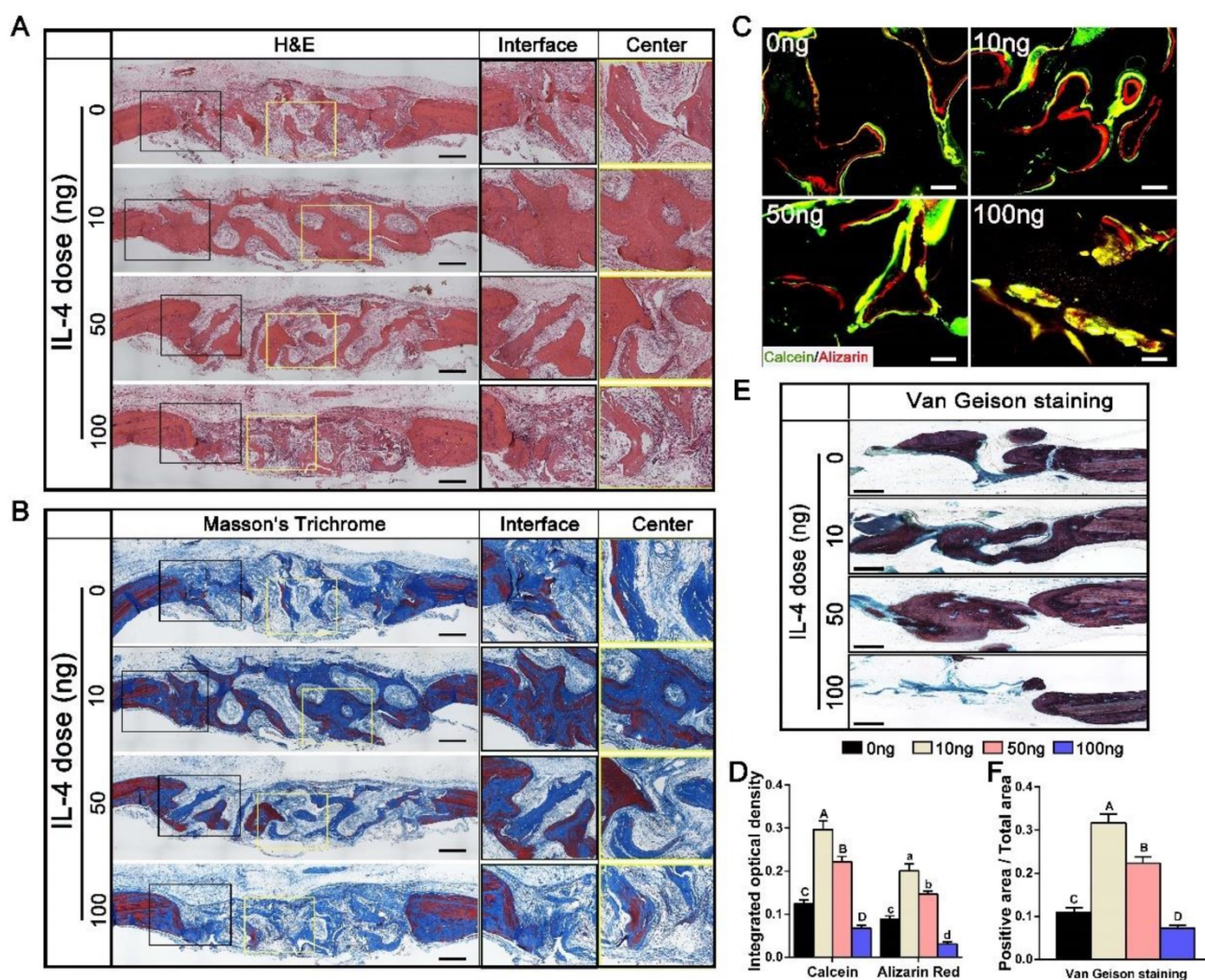


Figure 3. Histological evaluation of DBM regenerated bone tissue at 12 weeks after accurate and proactive immunomodulation via four different doses of IL-4 (0 ng, 10 ng, 50 ng and 100 ng). (A) H&E and (B) Masson's trichrome staining further confirmed the micro-CT findings that the 0 ng group exhibited a bone tissue in-growth pattern from peripheral region, while the 10 ng and 50 ng groups showed a bone tissue in-growth pattern from the peripheral region and an in-situ bone island formation pattern in the central region. However, the 100 ng group exhibited non-union healing, and the defects were filled with loose connective fibrous tissues surrounding the minimal new bone formation. Bar = 500 μ m. (C) Fluorescent images of newly formed bone double-labeled with calcein (green) and alizarin (red). Bar = 100 μ m. (D) Summary of fluorescence labeling. (E) Van Geison staining for new bone formation (red particles). Bar = 500 μ m. (F) Summary of Van Geison staining results. For all charts, the groups designated by different uppercase letters or lowercase letters were significantly different ($p < 0.05$).

Evaluation of the local inflammatory patterns after accurate and proactive immunomodulation via IL-4

TNF- α is primarily generated by M1 macrophages [22, 33], whereas IL-10 is secreted by M2 macrophages and displays potent anti-inflammatory properties [20]. Accordingly, TNF- α and IL-10 expression in the DBM and surrounding tissues was examined to further investigate the effect of IL-4 on inflammatory mediators. Consistent with the previous macrophage co-immunolabeling results, a low level of IL-10 and high level of TNF- α was detected in the 0 ng control group at 7 days. After the addition of IL-4, immunohistochemistry revealed that the secretion of IL-10 was increased (Figure 5A). However, the secretion of TNF- α at 7 and 14 days was

decreased after the addition of 10 ng and 50 ng IL-4 compared with the 0 ng control (Figure 5B).

A TUNEL assay was used to verify the influence of macrophage polarization on *in situ* tissue apoptosis, which is an important manifestation of the foreign body response [34, 35]. A recent study showed that IL-4 induced an anti-inflammatory and tissue repair program only when combined with apoptotic cells [36]. A relatively low level of apoptosis was observed at 7 and 14 days after implantation, regardless of IL-4 addition. Importantly, our results revealed that low doses IL-4 (10 and 50 ng) reduced tissue apoptosis at day 7 when compared with the 0 ng control, and apoptotic debris was completely cleared at day 14 (Figure 5C). This effect was not observed in the 100 ng group. Although the tissue apoptosis level was relatively low in the 100 ng group at day 7, the

TUNEL results revealed prolonged tissue apoptosis in the 100 ng group, and clearance of apoptotic debris was not apparent at day 14. In addition, the expression of cleaved-Caspase 3 in tissue sections was

detected by immunohistochemistry staining (Figure 5D), and the results were consistent with the TUNEL assay results.

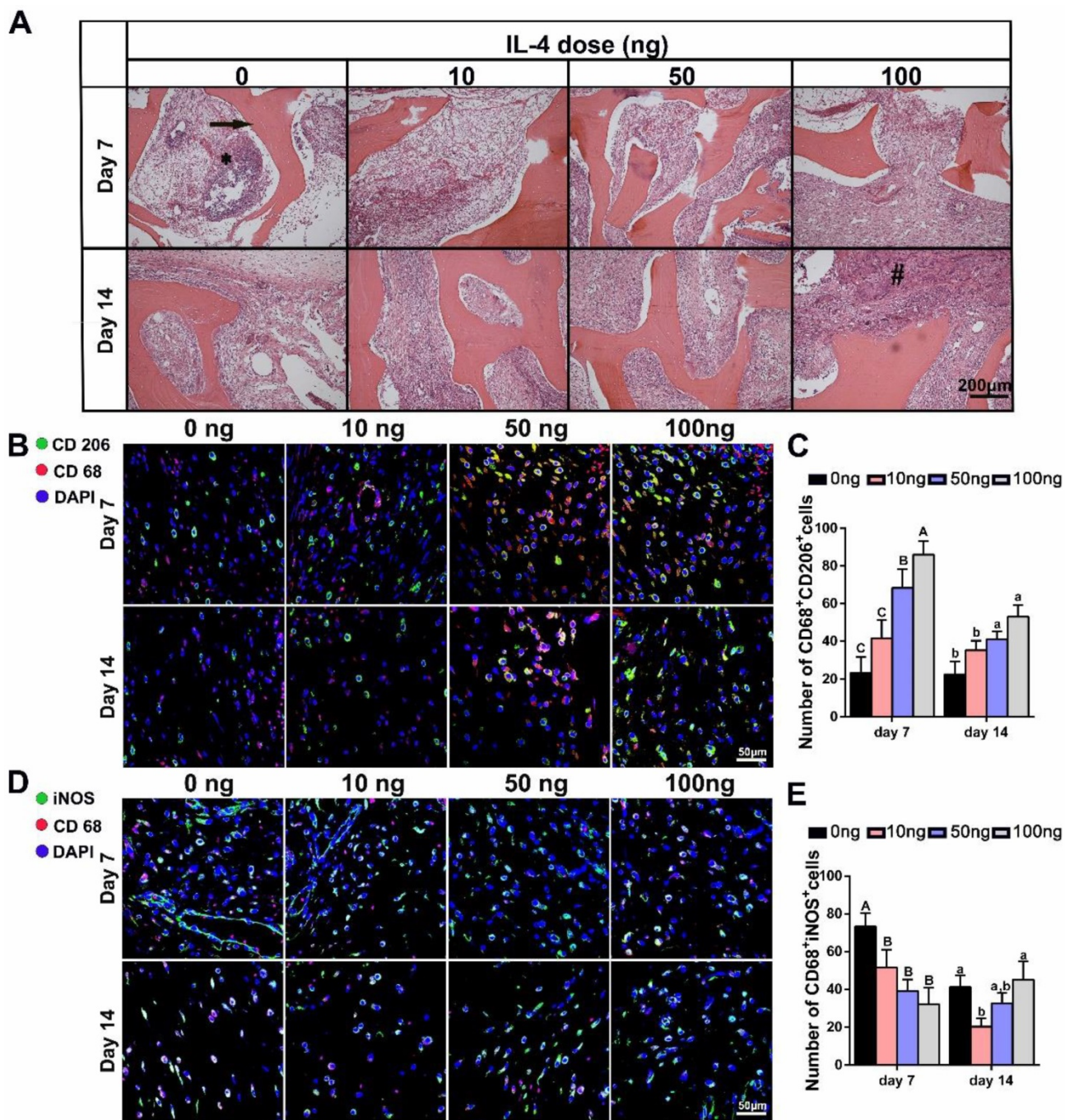


Figure 4. The effect of local addition of IL-4 on early-stage host response and M1/M2 macrophage polarization. Four doses of IL-4 (0 ng, 10 ng, 50 ng and 100 ng) were used. (A) H&E stained tissue sections from the interface of the undegraded demineralized bone matrix (arrow) at 7 days (top panel) and 14 days (bottom panel). * inflammatory cell infiltration; # foreign body giant cells. (B, D) Fluorescence microscopy images of (B) CD68 (red) and CD206 (green) co-immunolabeling, and (D) CD68 (red) and iNOS (green) co-immunolabeling to assess the phenotypic profiles of macrophages; DAPI was used to stain the cell nuclei. (C, E) Summary analysis of (C) CD68⁺CD206⁺ and (E) CD68⁺iNOS⁺ cells. For all charts, the groups designated by different uppercase letters or lowercase letters were significantly different ($p < 0.05$).

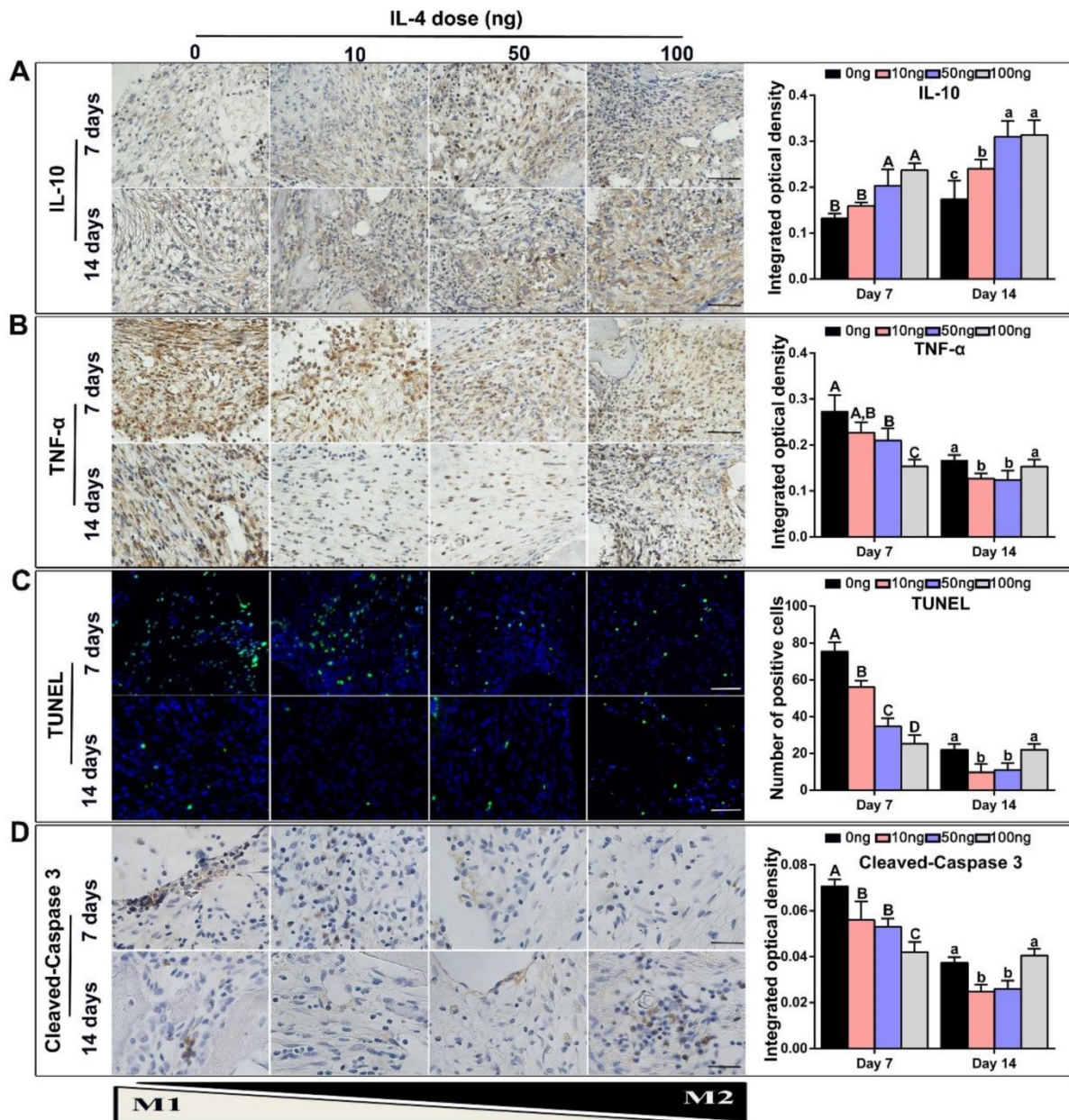


Figure 5. Accurate and proactive immunomodulation via IL-4 induced an anti-inflammatory host response accompanied by a reduction in local tissue cell apoptosis at the early stage of DBM implantation. Four doses of IL-4 (0 ng, 10 ng, 50 ng and 100 ng) were used. (A-B) Immunohistochemistry assay of the DBM and surrounding tissues at 7 and 14 days for the secretion of (A) IL-10 and (B) TNF- α . (C) TUNEL assay to assess apoptosis in the tissue surrounding the material. Apoptotic cells exhibit green fluorescence. (D) Representative images and summary of immunohistochemical staining of cleaved-Caspase 3. Bar = 200 μ m. For all charts, the groups designated by different uppercase letters or lowercase letters were significantly different ($p < 0.05$).

Evaluation of early-stage stem cell migration and osteogenic differentiation after accurate and proactive immunomodulation via IL-4

To further verify the effect of accurate and proactive immunomodulation in promoting bone regeneration, immunohistochemical staining for SSEA-4 was performed 7 days after surgery to identify mesenchymal stem cells (MSCs) that had migrated to the defect [37, 38]. The DBM scaffolds loaded with 10 ng IL-4 attracted more MSCs (SSEA-4-positive cells) than the other three groups

(Figure 6A, B). Consistent with the bone regeneration outcome, the number of SSEA-4-positive cells in the 100 ng group was lower than that in the other three study groups. Furthermore, the expression of the osteogenic transcription factor Runx2 and osteogenic marker OCN (indicators of cell commitment to an osteogenic lineage) was far more abundant in the 10 ng group than in the 0 and 100 ng groups 14 days after surgery (Figure 6C-F). These results indicated that accurate and proactive immunomodulation post-implantation of DBM could effectively enhanced stem cell migration and osteogenic differentiation.

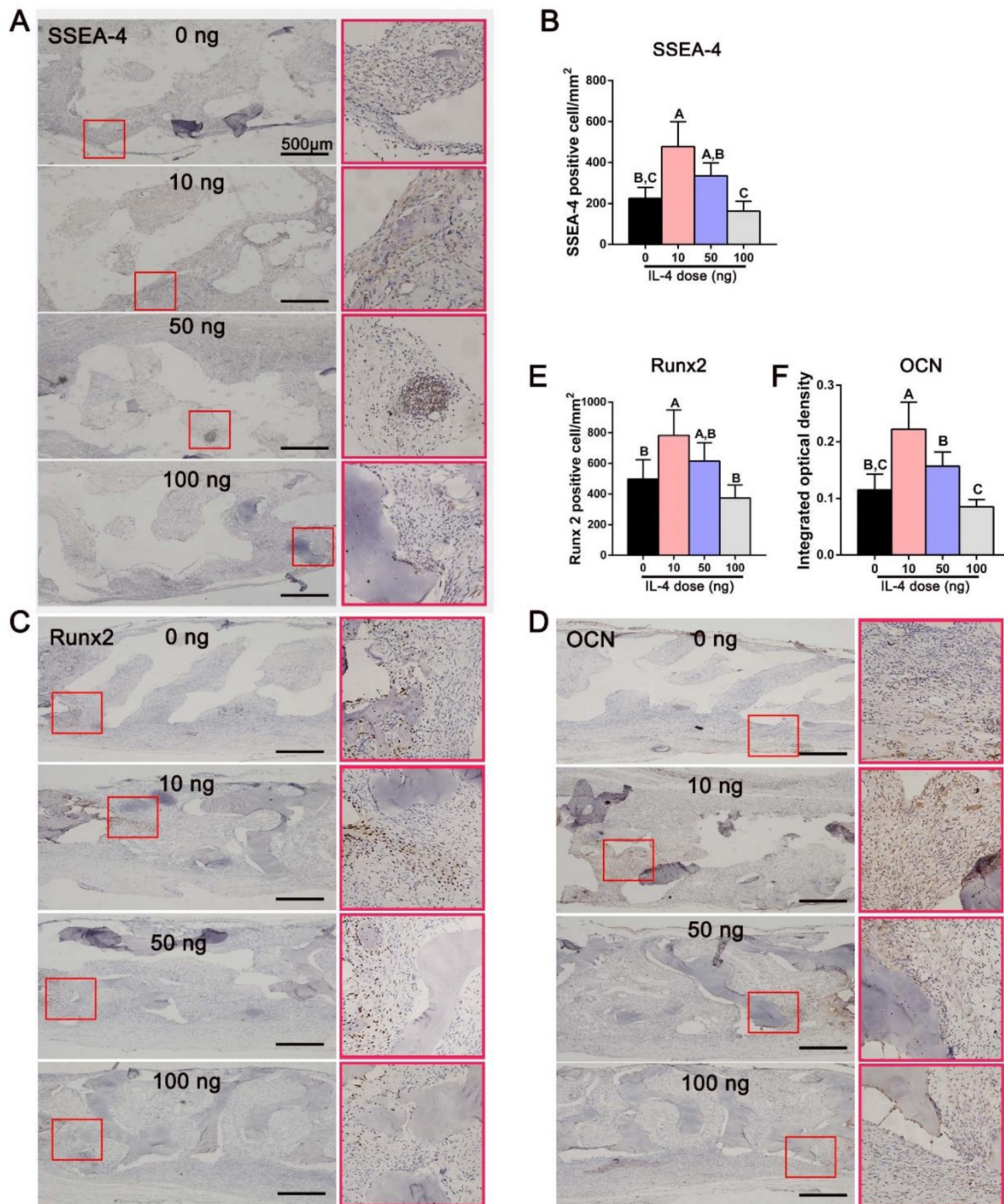


Figure 6. Accurate and proactive immunomodulation via IL-4 enhanced MSC migration and osteogenic differentiation at the early stage of DBM implantation. (A) The expression of SSEA-4 in the defect area 7 days after surgery. Immunohistochemical images showing significantly more MSCs (SSEA-4⁺) in the 10 ng group than in the other three groups. (B) Quantitative analysis of the number of SSEA-4⁺ cells. (C-D) The expression of (C) Runx2 and (D) OCN in the defect area 14 days after surgery. Immunomodulation via 10 ng of IL4 performed the best in upregulating expression levels of the osteogenic markers Runx2 and OCN. (E-F) Quantitative analysis of (E) the number of Runx2⁺ cells and (F) the mean integral optical density of OCN expression. For all charts, the groups designated by different uppercase letters were significantly different ($p < 0.05$).

Derivation and characteristics of M1 and M2 polarized macrophages *in vitro*

Potential communication events between polarized macrophages and osteogenesis and angiogenesis pathways were further examined using

conditioned media from polarized RAW cells. Immunofluorescence staining was first used to confirm the markers used as robust indicators of macrophage phenotypes. iNOS was expressed more strongly in M1 macrophages, and CD206 was

expressed in M2 phenotype (Figure 7A). Gene expression analysis further revealed that the M1 markers TNF- α , IL-1 β and IL-6 were highest in IFN γ - and LPS-induced macrophages and the M2 markers CD206, resistin-like molecule alpha (Retnl- α) and arginase-1 (Arg-1) were highest in IL-4-induced macrophages (Figure 7B). The cytokine secretion

characteristics of polarized macrophages were subsequently investigated. Expression of the pro-inflammation factor TNF- α was significantly increased in M1 macrophage medium, while the anti-inflammation factor IL-10 was increased in M2 macrophage medium (Figure 7C), confirming their polarization.

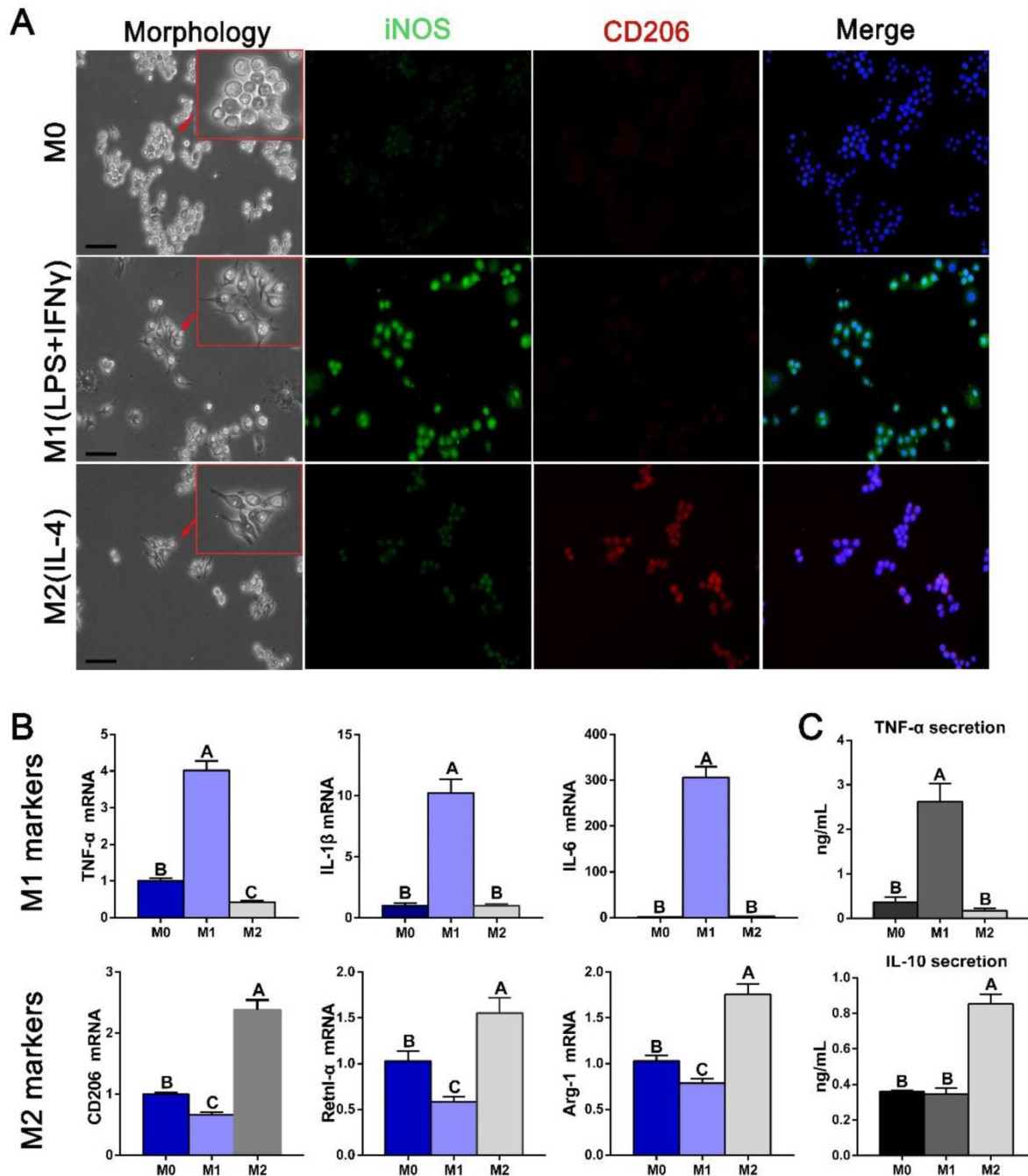


Figure 7. Derivation and characteristics of macrophages. (A) The morphology of polarized macrophages and fluorescence immunolabeling results for an M1 marker (iNOS) and M2 marker (CD206). Bar = 10 μ m. (B) Gene expression of some known markers of macrophage phenotypes. (C) ELISAs of the macrophage-conditioned media to examine the inflammatory and anti-inflammatory protein secretion levels. For all charts, the groups designated by different uppercase letters were significantly different ($p < 0.05$).

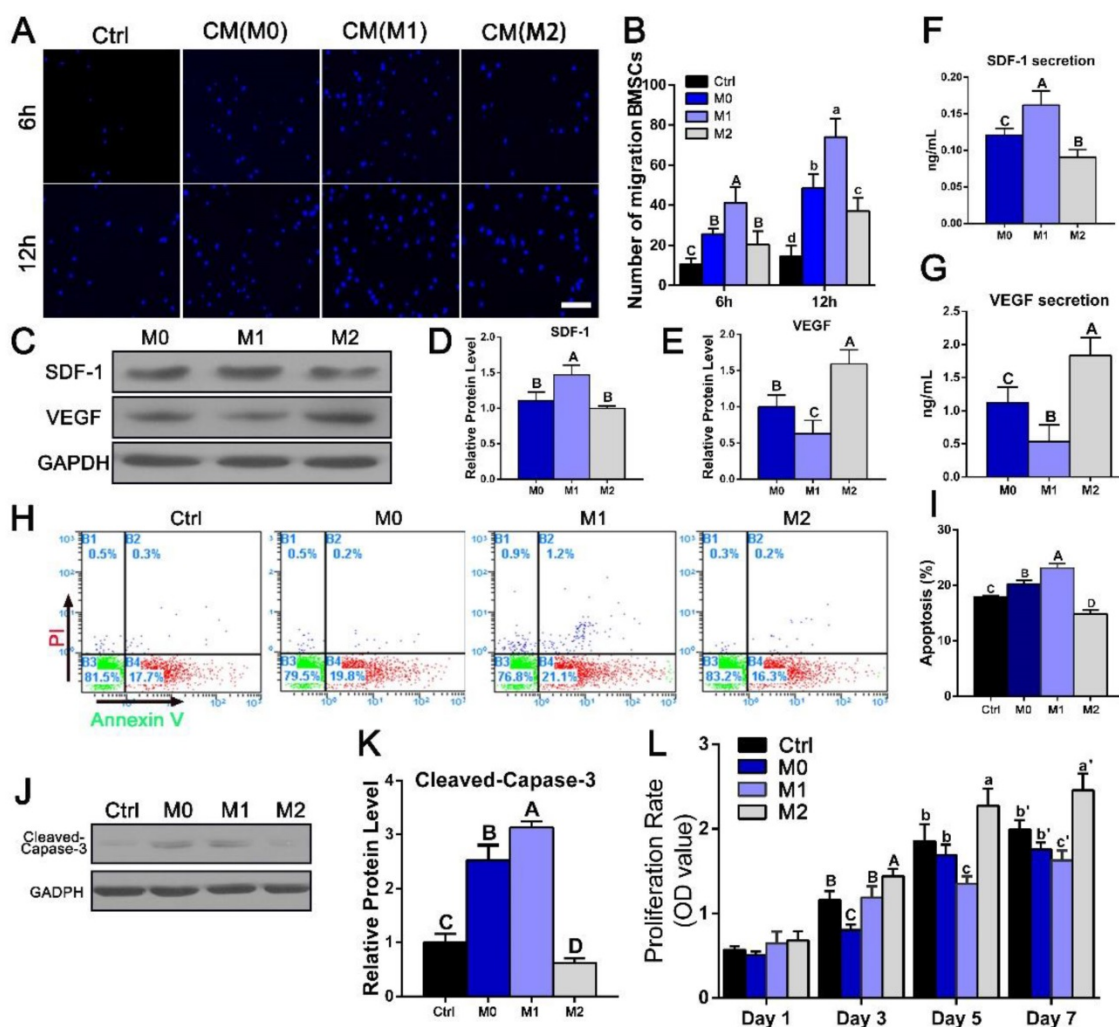


Figure 8. Assessment of BMSC migration, apoptosis and proliferation after culture with conditioned media (CMs) from the polarized macrophages. (A) Images of migrated BMSCs exposed to different CMs from M0, M1 and M2 macrophages at 6 h and 12 h. Bar = 100 μ m. (B) Summary of BMSC migration. (C) Western blotting of SDF-1 and VEGF secretion by different macrophage phenotypes. (D-E) Quantification analysis of the expression of (D)SDF-1 and (E)VEGF. (F-G) ELISAs of CMs secreted by different macrophage phenotypes to assess the secretion levels of (F) SDF-1 and (G) VEGF proteins. (H) Representative images of BMSC apoptosis detected with Annexin V-FITC/propidium iodide at day 3 after culture with different CMs. (I) Summary of BMSC apoptosis. (J) Western blot of cleaved-Caspase-3 activity. (K) Quantification analysis of the expression of cleaved-Caspase-3. (L) Cell proliferation after 1, 3, 5 and 7 days of incubation with different CMs was measured with CCK8 assays. For all charts, the groups designated by different uppercase letters or lowercase letters were significantly different ($p < 0.05$).

Effects of polarized macrophages on BMSC migration, proliferation and osteogenic differentiation *in vitro*

Next, we investigated the role of different macrophage phenotypes in promoting migration, proliferation and osteogenic differentiation of BMSCs. We first evaluated the effect of different RAW-conditioned media on the cell migration and proliferation characteristics of BMSCs. BMSC migration increased significantly in the presence of culture medium from M1 macrophages (1.51-5.1 fold, $p < 0.05$) compared with that from the other groups (Figure 8A, B). The expression of SDF-1, which has been reported to induce cell migration, was also evaluated in the polarized macrophages (Figure 8C, D, F). Consistent with the migration results, the SDF-1 expression level was significantly elevated in the M1

macrophages.

The effects of conditioned medium from different macrophage phenotypes on the viability and proliferation characteristics of BMSCs were then examined. BMSC apoptosis was detected with Annexin V-FITC/propidium iodide double staining, and typical figures for the flow cytometric analyses are presented in Figure 8H. More apoptotic cells were observed after culture with M1-conditioned medium than after culture with control medium, while the apoptotic rate in the M2 group ($14.9 \pm 0.71\%$) was significantly reduced compared with that in the M1 group ($23.1 \pm 0.85\%$, $p < 0.05$) (Figure 8I). Western blotting results further revealed that the M2 phenotype medium significantly reduced cleaved-Caspase-3 activation after 3 days of culture (Figure 8J, K). Cell proliferation during 7 days of incubation was assessed using a CCK8 assay. No

significant differences were noted between the groups at day 1 ($p > 0.05$) (Figure 8L). At day 3, cell viability was statistically increased in the M2 group compared with the M0 and the M1 groups, and this difference became more obvious after 7 days of culturing. These results indicated that IL-4-induced M2 macrophages were beneficial for the viability and proliferation of BMSCs ($p < 0.05$).

BMSC osteogenic differentiation was induced by culturing the cells in different conditioned media with osteogenic supplements. ALP staining at 7 days and AR staining and immunofluorescence staining of OCN and Runx-2 at 14 days indicated that M2 macrophages were beneficial for BMSC osteogenesis, whereas M1 macrophages clearly inhibited osteogenic differentiation (Figure 9A). Moreover, the quantitative data for ALP activity and AR staining

presented in Figure 9B agree with these effects of the macrophage subsets on BMSC osteogenesis. Consistent with these results, osteoblast marker genes, including ALP, COL1, OPN, RUNX2, BMP-2 and OCN were examined at 7 and 14 days. The transcription of osteoblast marker genes was prominently increased by M2 type macrophages, whereas M1 type macrophages demonstrated the opposite results ($p < 0.05$) (Figure 9C). Since previous studies have reported that inflammatory cytokines influence BMSC osteogenic differentiation [39], we also evaluated whether IL-4 has a direct effect on the osteogenic ability of BMSCs. We treated BMSC monocultures with IL-4 after seeding, and observed no significant differences in AR staining between BMSCs cultured with or without IL-4 in either growth medium or osteogenic induction medium (Figure S2).

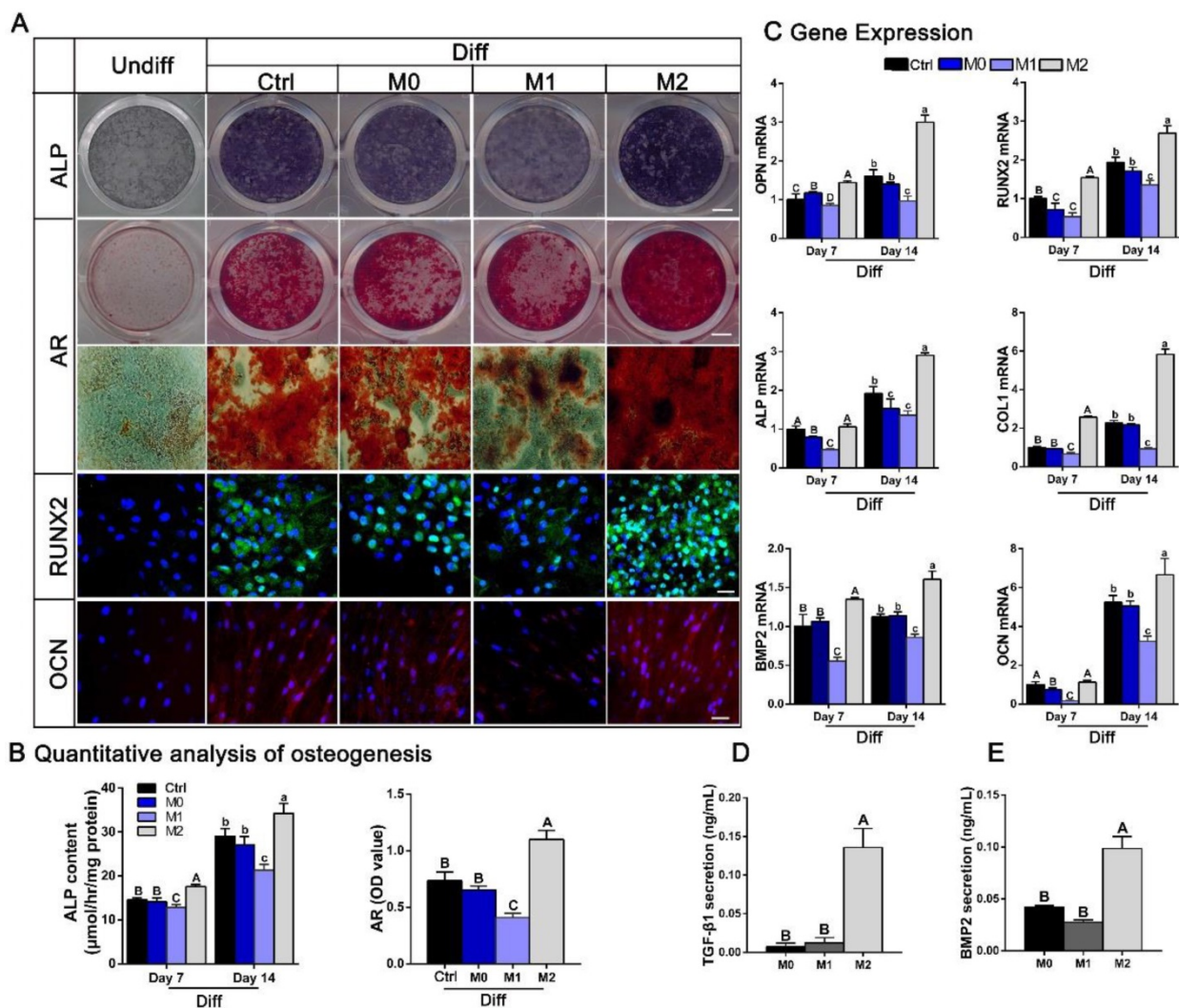


Figure 9. The effect of different conditioned media (CMs) from polarized macrophages on osteogenic differentiation of BMSCs. (A) Images of ALP and AR staining and fluorescence immunolabeling of BMSCs after culture in CMs from M0, M1 and M2 macrophages when subjected to osteogenic supplements. Undiff: BMSCs cultured in standard medium only. Diff: osteogenic medium. Bar = 3 mm for entire plate views. Bar = 50 μm for fluorescence images. (B) Quantitative evaluation of ALP activity at day 7 and day 14 and quantification of the AR staining results at day 14. (C) Real-time qPCR analyses of ALP, COL1, OPN, RUNX2, BMP2 and OCN mRNA expression in BMSCs at day 7 and day 14. (D-E) ELISAs of CMs from M0, M1 and M2 macrophages to assess the levels of osteogenic (D) TGF-β1 and (E) BMP2 secretion. For all charts, the groups designated by different uppercase letters or lowercase letters were significantly different ($p < 0.05$).

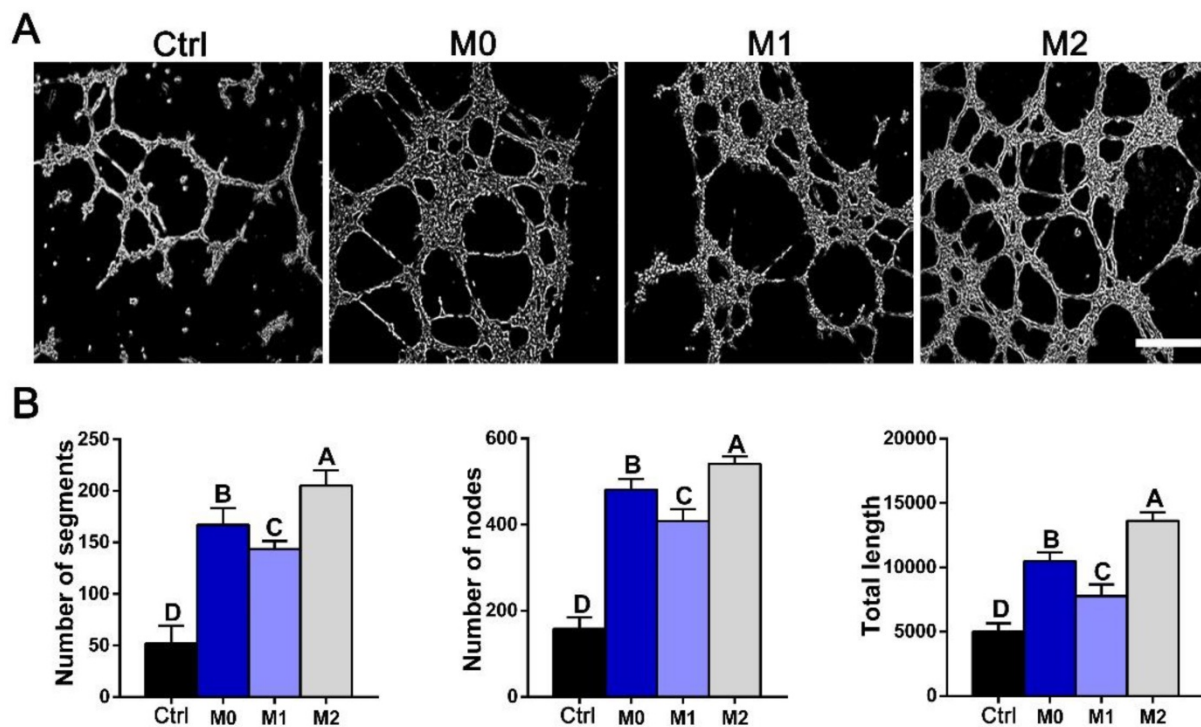


Figure 10. *In vitro* tube formation. (A) Tube formation of HUVECs exposed to control DMEM (Ctrl) or conditioned mediums from M0, M1 and M2 macrophages for 12 h. Bar = 100 μ m. (B) Summary of tube formation. For all charts, the groups designated by different uppercase letters were significantly different ($p < 0.05$).

We then sought to elucidate potential cytokines responsible for the increased osteogenic differentiation observed after cultured with conditioned medium from M2 macrophages. Since TGF- β and BMP signaling have widely recognized roles in osteogenic differentiation and bone formation, secretion of the cytokines BMP-2 and TGF- β 1 by polarized macrophages was investigated. ELISA analysis of the conditioned mediums showed that the concentration of the osteogenic factors BMP-2 and TGF- β 1 were significantly increased in condition medium from M2 macrophages compared with that from M0 or M1 macrophages ($p < 0.05$) (Figure 9D-E).

Taken together, our observations suggest that conditioned medium from M1 macrophages facilitates BMSC migration, while conditioned medium from M2 macrophages significantly increases BMSC viability, proliferation and differentiation.

Effect of polarized macrophages on *in vitro* angiogenesis

To assess the functional role of macrophage-secreted factors in angiogenesis, an *in vitro* sprouting assay was performed. HUVECs organized into networks with significantly more sprouts and greater total length in conditioned medium from M2 macrophages than in medium from M1 macrophages (Figure 10). The trends in sprouting mirrored the macrophage secretion profiles of VEGF investigated by western blot and ELISA (Figure 8C, G).

Discussion and Conclusions

Recently, biomaterial-immune system interactions have been recognized as a crucial factor that influences material-mediated tissue regeneration [10, 16, 40]. In this study, we successfully developed a new strategy to accurately and proactively create a desirable host immune response via the addition of IL-4 (the M2 macrophage polarization cytokine), which enhanced bone substitute material-mediated healing and regeneration. The present study provided evidence from both *in vivo* and *in vitro* findings regarding the potential profound influence of immunomodulation patterns on the osteogenesis and angiogenesis patterns during bone defect healing (Figure 11). It has been demonstrated that accurate immunomodulation is a prerequisite for promoting material-mediated rapid and homogeneous vascularization and osteogenesis and likely holds great promise in the context of bone substitute material design.

To explore the effect of an accurate and proactive immunomodulatory strategy on bone substitute material-mediated bone regeneration, DBM was chosen as the model material, and the bioactive factors in DBM, such as BMP-2 and TGF- β , were destroyed to eliminate its inherent osteoinductive effects. Given that inflammation is a crucial factor influencing regeneration, we envisioned a new

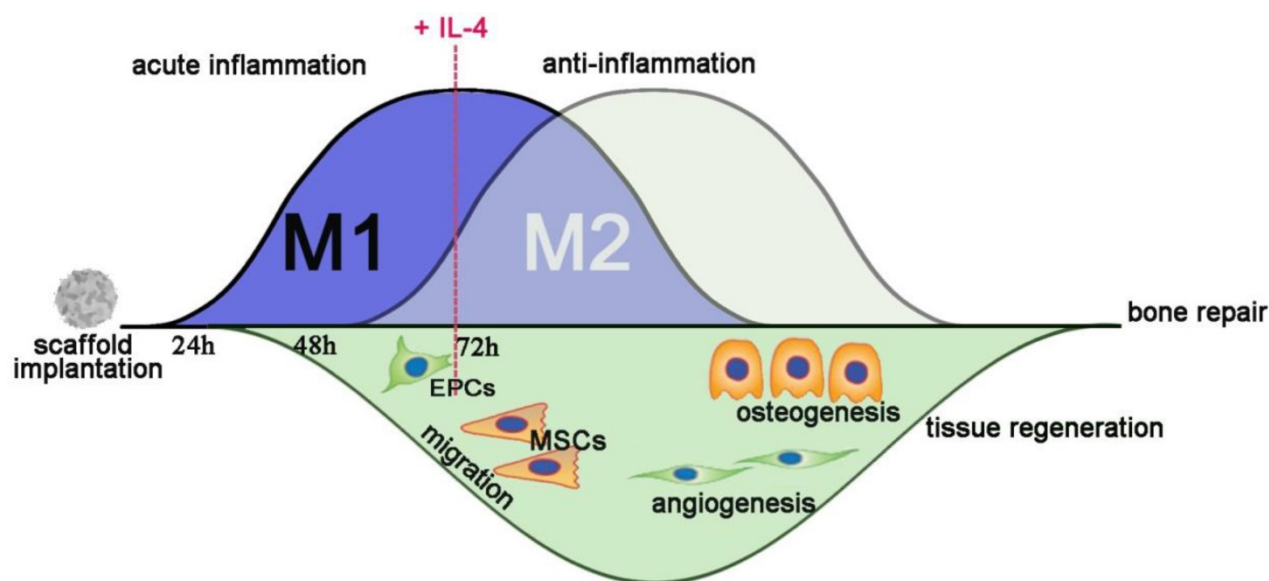


Figure 11. Schematic of how accurate and proactive inflammatory modulation via IL-4 improved bone regeneration and angiogenesis. EPCs: endothelial progenitor cells; MSCs: mesenchymal stem cells.

strategy to proactively and accurately optimize the host inflammatory microenvironment after DBM implantation, and successfully treated a large bone defect with bone-like tissue that integrated into the defect.

Acute inflammation is the first stage of tissue healing [41], and anti-inflammatory strategies during this stage are often associated with delayed healing [42-45]. M1 macrophages have traditionally been regarded as professional phagocytes that clear debris and bacterial pathogens [46]. Evidence is emerging to support a broader role of M1 macrophages in orchestrating the downstream inflammatory cascade [47]. Therefore, the timing of the local delivery of IL-4 was delayed to 3 days post-implantation, when, which is the time in normal bone healing at which the inflammatory cytokines levels start to decline [48, 49]. Daily injection of IL-4 was performed from day 3 to day 7, since it was reported that sustained delivery of anti-inflammatory agents is beneficial for injury tissue repair [1, 18]. Furthermore, how to accurately modulate the host immune response is another important issue. Although recent studies support the notion that macrophage polarization into the M2 phenotype is beneficial for bone formation [17], excessive M2 type polarization has also been reported to induce pro-fibrotic effects and promote macrophages fusion into foreign body giant cells *in vitro* and *in vivo* [50, 51]. Consequently, four different doses (0, 10, 50 and 100 ng) of IL-4, the M2-polarizing cytokine, were used to accurately modulate the host inflammatory microenvironment. We hypothesized that the accurate and proactive promotion of the anti-inflammatory response after acute inflammation

would further optimize the immunomodulatory effect and enhance the bone substitute material-mediated osteogenesis and related angiogenesis.

The bone defect regeneration processes in cranial bone defect were investigated in our study. However, different bone regeneration and angiogenesis patterns were observed via micro-CT and histological analyses after treatment with different doses of IL-4. In the 10 ng group, the defects were completely bridged with bone-like tissue. In the 50 ng group, newly formed bone-like tissue bridged both ends of the bone defects, but the number of bone formation islands inside the scaffold center was less than that in the 10 ng group, followed by the 0 ng group, and the least bone formation was found in the 100 ng group. Bone formation islands in the 100 ng group sporadically crept from both ends of the bone defect. The difference in bone regeneration patterns was closely correlated with the different angiogenic patterns, especially the spatial distribution of the vascular networks. The 10 ng group exhibited significantly more vascular network formation than the other groups both in the central and peripheral regions. This finding was likely observed because the osteogenic and angiogenic processes are highly interdependent during bone defect repair [6]. Immunomodulation properties were subsequently compared among the groups treated with different IL-4 doses via immunofluorescence and immunohistochemistry analyses. The lower number of M2 macrophages surrounding the 0 ng group defects suggests their involvement in the limited bone regeneration induced by the DBM scaffold alone. Importantly, accurate and proactive

immunomodulation with low-dose IL-4 (10 ng) outperformed the other groups in neo-vascularization and osteogenesis. The 10 ng group generated more bone tissue than the other groups, achieved successful bridging of defects and exhibited infiltration of the defect by a substantial number of blood vessels. However, the primarily M2 response (100 ng) led to chronic inflammation and the formation of fibrous tissue around the material compared with the control. Thus, this study further confirmed that the osteogenic and angiogenic processes are intimately linked with the inflammatory response during bone defect treatment [19, 22] and accurate and proactive immunomodulation is pivotal for the development of a suitable bone substitute material.

Previous gain and loss studies confirmed the crucial role of macrophages in directing host inflammatory and immune processes after injury [52-54]. When IL-4 was not added, the number of M1 macrophages in tissues around the DBM scaffold decreased from 7 days to 14 days, indicating the good biocompatibility of DBM. However, traditional bone substitute materials are relatively "inert" and do not have immunomodulatory properties [1], and the number of M2 macrophages around the DBM scaffold (in the absence of IL-4 treatment) stayed at a low level during this time frame. With the addition of specific dose of IL-4 (10 ng), a preferable anti-inflammatory and pro-healing microenvironment was created, and the bone regeneration in cranial defects was improved. Proper M2 response at the biomaterial interface via low-dose IL-4 could favor anti-inflammatory conditions with increased secretion of IL-10 and reduced TNF- α expression in tissues around the material [36]. Our results also revealed that apoptotic cells were rapidly cleared within 2 weeks when the inflammatory microenvironment was accurately modulated. These findings are important manifestations of the resolution of inflammation [34], resulting in improved osteointegration and osteogenesis at 12 weeks post-implantation. Conversely, high-dose IL-4 (100 ng), which induced high expression of M2 macrophage markers, led to fibrosis formation. This finding may be due to disruption of the M1/M2 balance. These results are consistent with previous findings showing that IL-4 is required for *in vitro* foreign body giant cell formation [50], and undue M2 polarization would result in fibrosis formation [51]. Additionally, a reduction in M1 polarization was revealed after IL-4 delivery. Hachim et al. [18] also reported an increase in M2 macrophages accompanied by a reduction in M1 macrophages with IL-4-loaded polypropylene meshes. Disruption of the M1/M2 balance may account for the delayed tissue inflammation and

apoptosis observed after 14 days, resulting in impaired bone regeneration. Taken together, the collective data from the present study suggest that bone regeneration is closely related to immunomodulation patterns, and if the M1/M2 balance is pushed excessively toward either M1 or M2, then vascularization and bone regeneration cannot be achieved.

Bone formation occurs through a process of cell migration, proliferation and maturation [55]. In response to chemoattractant factors, stem cells and endothelial progenitor cells are recruited by direct migration from their local niches, and then the recruited cells proliferate and develop into mature bone tissues and vessels, respectively [56]. The present study provided evidence from findings both *in vivo* and *in vitro* for a contribution of coordinated M1 and M2 polarization to the robust promotion of bone formation. MSCs from the neighboring tissue rapidly migrated into the scaffolds and differentiated into an osteogenic lineage to fill the defects after accurate and proactive immunomodulation. M1 macrophages are known to secrete factors that are well-described to initiate the process of migration, including SDF-1, while M2 macrophages secrete factors known to be involved in promoting *in vitro* osteogenesis and angiogenesis at later stages, along with the liberation of cytokines, including BMP-2, BMP-4, VEGF and TGF- β 1 [1, 57]. It is reported that the sequential release of SDF-1 and BMP-2 from biomaterial scaffolds enhances bone regeneration [58], suggesting that coordinated activation of M1 and M2 macrophages, which secrete these two factors, would be beneficial. Here, we demonstrated that IL-4 induced macrophage polarization into an M2 type and had no direct effect on the osteogenic ability of BMSCs. The present study and previous studies [59, 60] show that the presence of M2 macrophages influences the effect of IL-4 and thereby enhances the osteogenic differentiation of BMSCs. These results may appear to be contradictory to those observing that increased osteogenesis can be induced with M1 macrophages [48, 60]. This may be attributed to the fact that the dynamic bi-directional cellular interactions between BMSCs and macrophages were ignored in these studies, which used a direct coculture system. After all, BMSCs can also promote macrophage differentiation toward an M2-like phenotype [61, 62]. Therefore, in this study the effects of macrophage type on the migration, proliferation and maturation of BMSCs were investigated through an indirect co-culture model using conditioned media. Specifically, the present study demonstrated that M1 macrophages significantly promoted BMSC migration and M2 polarization showed stimulatory

effects on BMSC proliferation and osteogenesis.

Despite these encouraging results, translating this accurate and proactive immunomodulatory strategy into a biomaterial design has to be pursued in further studies. Although the calvarial bone regeneration outcome provides evidence that sustained administration of 10 ng of IL-4 via local injection is effective for *in vivo* use, further work should investigate how to endow bone substitute materials with the ability to accurately and proactively release IL-4 directly from the biomaterial.

In summary, as a proof-of-concept experiment, we used four different doses of IL-4 to proactively explore the effects of accurate immunomodulation on bone substitute material-based bone regeneration. As expected, our *in vivo* data demonstrated that proper delivery of IL-4 can generate the most preferable M1/M2 macrophage profile, resulting in a pro-healing microenvironment coupled with enhanced downstream osteogenesis and angiogenesis. Moreover, *in vitro* data suggest that the coordinated involvement of M1 (chemotactic effects) and M2 (mitogenic and morphogenic effects) macrophages promotes bone osteogenesis, explaining the *in vivo* findings. With the help of drug delivery systems, this accurate and proactive immunomodulatory strategy holds great promise for construct clinically effective bone substitute material with accurate and sustained delivery of IL-4.

Abbreviations

ALP: alkaline phosphatase; AR: alizarin red; BMSCs: bone mesenchymal stem cells; DBM: decellularized bone matrix; iNOS: inducible nitric oxide synthase; TUNEL: terminal deoxynucleotidyl transferase 2'-deoxyuridine 5'-triphosphate nick end labeling; LPS: lipopolysaccharide; BMD: bone mineral density; OPN: osteopontin; RUNX2: runt-related transcription factor 2; BMP-2: bone morphogenetic protein-2; OCN: osteocalcin.

Supplementary Material

Supplementary figures and tables.

<http://www.thno.org/v08p5482s1.pdf>

Acknowledgements

This work was supported by National Key R&D Program of China (2016YFC1100100), National Natural Science Foundation of China (81772354, 81572137, 81371964, 81771042), National Young Thousand-Talent Scheme to Zhang Zhi-Yong.

Competing Interests

The authors have declared that no competing interest exists.

References

- Chen Z, Klein T, Murray RZ, Crawford R, Chang J, Wu C. et al. Osteoimmunomodulation for the development of advanced bone biomaterials. *Materials Today*. 2016;19:304-21.
- Tang D, Tare RS, Yang LY, Williams DF, Ou KL, Oreffo RO, Biofabrication of bone tissue: approaches, challenges and translation for bone regeneration. *Biomaterials*. 2016;83:363-82.
- Wang X, Xu S, Zhou S, Xu W, Leary M, Choong P. et al. Topological design and additive manufacturing of porous metals for bone scaffolds and orthopaedic implants: A review. *Biomaterials*. 2016;83:127-41.
- Ayala R, Zhang C, Yang D, Hwang Y, Aung A, Shroff SS. et al. Engineering the cell-material interface for controlling stem cell adhesion, migration, and differentiation. *Biomaterials*. 2011;32:3700-11.
- Hollister SJ. Porous scaffold design for tissue engineering. *Nature materials*. 2005;4:518-524.
- Wang L, Zhu LX, Wang Z, Lou AJ, Yang YX, Guo Y, et al. Development of a centrally vascularized tissue engineering bone graft with the unique core-shell composite structure for large femoral bone defect treatment. *Biomaterials*. 2018;175:44-60.
- Vishwakarma A, Bhise NS, Evangelista MB, Rouwkema J, Dokmeci MR, Ghaemmaghami AM. et al. Engineering Immunomodulatory Biomaterials To Tune the Inflammatory Response. *Trends in biotechnology*. 2016;34:470-82.
- Shi M, Chen Z, Farnaghi S, Friis T, Mao X, Xiao Y. et al. Copper-doped mesoporous silica nanospheres, a promising immunomodulatory agent for inducing osteogenesis. *Acta Biomaterialia*. 2016;30:334-44.
- Wynn TA, Vannella KM. Macrophages in Tissue Repair, Regeneration, and Fibrosis. *Immunity*. 2016;44:450-62.
- Zhang W, Zhao F, Huang D, Fu X, Li X, Chen X. Strontium-Substituted Submicrometer Bioactive Glasses Modulate Macrophage Responses for Improved Bone Regeneration. *ACS applied materials & interfaces*. 2016;8:30747-58.
- Wu C, Xia L, Han P, Xu M, Fang B, Wang J. et al. Graphene-oxide-modified β -tricalcium phosphate bioceramics stimulate *in vitro* and *in vivo* osteogenesis. *Carbon*. 2015;93:116-29.
- Chen Z, Ni S, Han S, Crawford R, Lu S, Wei F. et al. Nanoporous microstructures mediate osteogenesis by modulating the osteo-immune response of macrophages. *Nanoscale*. 2016;9:706.
- Sun JL, Jiao K, Niu LN, Jiao Y, Song Q, Shen J. et al. Intrafibrillar silicified collagen scaffold modulates monocyte to promote cell homing, angiogenesis and bone regeneration. *Biomaterials*. 2017;113:203-16.
- Wu C, Chen Z, Wu Q, Yi D, Friis T, Zheng X. et al. Clinostatite coatings have high bonding strength, bioactive ion release, and osteoimmunomodulatory effects that enhance *in vivo* osseointegration. *Biomaterials*. 2015;71:35-47.
- Laschke MW, Harder Y, Amom M, Martin I, Farhadi J, Ring A. et al. Angiogenesis in tissue engineering: breathing life into constructed tissue substitutes. *Tissue engineering*. 2016;12:2093-104.
- Zhang Q, Hubenak J, Iyyanki T, Alfred E, Turza KC, Davis G. et al. Engineering vascularized soft tissue flaps in an animal model using human adipose-derived stem cells and VEGF+PLGA/PEG microspheres on a collagen-chitosan scaffold with a flow-through vascular pedicle. *Biomaterials*. 2015;73:198-213.
- Hu Z, Ma C, Rong X, Zou S, Liu X. Immunomodulatory ECM-like microspheres for accelerated bone regeneration in diabetes mellitus. *ACS Applied Materials & Interfaces*. 2018;10:2377-90.
- Hachim D, LoPresti ST, Yates CC, Brown BN. Shifts in macrophage phenotype at the biomaterial interface via IL-4 eluting coatings are associated with improved implant integration. *Biomaterials*. 2016;112:95-107.
- Spiller KL, Nassiri S, Witherell CE, Anfang RR, Ng J, Nakazawa KR. et al. Sequential delivery of immunomodulatory cytokines to facilitate the M1-to-M2 transition of macrophages and enhance vascularization of bone scaffolds. *Biomaterials*. 2015;37:194-207.
- Wan J, Benkdane M, Teixeira-Clerc F, Bonnafous S, Louvet A, Lafdil F. et al. M2 Kupffer cells promote M1 Kupffer cell apoptosis: a protective mechanism against alcoholic and nonalcoholic fatty liver disease. *Hepatology*. 2014;59:130-142.
- Spiller KL, Anfang RR, Spiller KJ, Ng J, Nakazawa KR, Daulton JW. et al. The role of macrophage phenotype in vascularization of tissue engineering scaffolds. *Biomaterials*. 2014;35:4477-88.
- Chan JK, Glass GE, Ersek A, Freidin A, Williams GA, Gowers K. et al. Low-dose TNF augments fracture healing in normal and osteoporotic bone by up-regulating the innate immune response. *EMBO Molecular Medicine*. 2015;7:547-61.
- Stein M, Keshav S, Harris N, Gordon S. Interleukin 4 potently enhances murine macrophage mannose receptor activity: a marker of alternative immunologic macrophage activation. *The Journal of experimental medicine*. 1992;176:287-92.
- Ruan J, Wang X, Yu Z, Wang Z, Xie Q, Zhang D. et al. Enhanced Physicochemical and Mechanical Performance of Chitosan-Grafted Graphene Oxide for Superior Osteoinductivity. *Advanced Functional Materials*. 2016;26:1085-97.
- Zhang W, Chang Q, Xu L, Li G, Yang G, Ding X. et al. Graphene Oxide-Copper Nanocomposite-Coated Porous CaP Scaffold for Vascularized Bone Regeneration via Activation of Hif-1alpha. *Advanced Healthcare Materials*. 2016;5:1299-309.

26. Grayson WL, Frohlich M, Yeager K, Bhumiratana S, Chan ME, Cannizzaro C. et al. Vunjak-Novakovic, Engineering anatomically shaped human bone grafts. *Proceedings of the National Academy of Sciences of the United States of America*. 2010;107:3299-304.
27. Wang ZX, Chen C, Zhou Q, Wang XS, Zhou G, Liu W. et al. The Treatment Efficacy of Bone Tissue Engineering Strategy for Repairing Segmental Bone Defects Under Osteoporotic Conditions. *Tissue Engineering Part A*. 2015;21:2346-55.
28. Moiola EK, Clark PA, Sumner DR, Mao JJ. Autologous stem cell regeneration in craniocostosis. *Bone*. 2008;42:332-40.
29. Ren Z, Wang Y, Ma S, Duan S, Yang X, Gao P. et al. Effective Bone Regeneration Using Thermosensitive Poly(N-Isopropylacrylamide) Grafted Gelatin as Injectable Carrier for Bone Mesenchymal Stem Cells. *ACS Applied Material & Interfaces*. 2015;7:19006-15.
30. Wang J, Wu D, Zhang Z, Li J, Shen Y, Wang Z. et al. Biomimetically Ornamented Rapid Prototyping Fabrication of an Apatite-Collagen-Polycaprolactone Composite Construct with Nano-Micro-Macro Hierarchical Structure for Large Bone Defect Treatment. *ACS applied materials & interfaces*. 2015;7:26244-56.
31. Feng YF, Wang L, Zhang Y, Li X, Ma ZS, Zou JW. et al. Effect of reactive oxygen species overproduction on osteogenesis of porous titanium implant in the present of diabetes mellitus. *Biomaterials*. 2013;34:2234-43.
32. Wang M, Yu Y, Dai K, Ma Z, Liu Y, Wang J. et al. Improved osteogenesis and angiogenesis of magnesium-doped calcium phosphate cement via macrophage immunomodulation. *Biomaterials science*. 2016;4:1574-83.
33. Lu Z, Wang G, Dunstan CR, Chen Y, Lu WY, Davies B. et al. Activation and promotion of adipose stem cells by tumour necrosis factor-alpha preconditioning for bone regeneration. *Journal of cellular physiology*. 2013;228:1737-44.
34. Bartsch I, Willbold E, Yarmolenko S, Witte F. *In vivo* fluorescence imaging of apoptosis during foreign body response. *Biomaterials*. 2012;33:6926-32.
35. Milde R, Ritter J, Tennent GA, Loesch A, Martinez FO, Gordon S. et al. Multinucleated Giant Cells Are Specialized for Complement-Mediated Phagocytosis and Large Target Destruction. *Cell reports*. 2015;13:1937-48.
36. Bosurgi L, Cao YG, Cabeza-Cabrero M, Tucci A, Hughes LD, Kong Y. et al. Macrophage function in tissue repair and remodeling requires IL-4 or IL-13 with apoptotic cells. *Science*. 2017;356:1072-6.
37. Zhang W, Zhu C, Wu Y, Ye D, Wang S, Zou D. et al. VEGF and BMP-2 promote bone regeneration by facilitating bone marrow stem cell homing and differentiation. *European Cells and Materials*. 2014;27:1-12.
38. Thevenot PT, Nair AM, Shen J, Lotf P, Ko C-Y, Tang L. The effect of incorporation of SDF-1 α into PLGA scaffolds on stem cell recruitment and the inflammatory response. *Biomaterials*. 2010;31:3997-4008.
39. Ciavarella C, Gallitto E, Ricci F, Buzzi M, Stella A, Pasquinelli G. The crosstalk between vascular MSCs and inflammatory mediators determines the pro-calcific remodelling of human atherosclerotic aneurysm. *Stem cell research & Therapy*. 2017;8:99.
40. Reeves AR, Spiller KL, Freytes DO, Vunjak-Novakovic G, Kaplan DL. Controlled release of cytokines using silk-biomaterials for macrophage polarization. *Biomaterials*. 2015;73: 272-83.
41. Marsell R, Einhorn TA. The biology of fracture healing. *Injury*. 2015;42:551-5.
42. Kolar P, Schmidt-Bleek K, Schell H, Gaber T, Toben D, Schmidmaier G. et al. The early fracture hematoma and its potential role in fracture healing. *Tissue Engineering Part B Reviews*. 2010;16:427-34.
43. Kolar P, Gaber T, Perka C, Duda GN, Buttgerit F. Human early fracture hematoma is characterized by inflammation and hypoxia. *Clinical orthopaedics and related research*. 2011;469:3118-26.
44. Hoff P, Maschmeyer P, Gaber T, Schutze T, Raue T, Schmidt-Bleek K. et al. Human immune cells' behavior and survival under bioenergetically restricted conditions in an *in vitro* fracture hematoma model. *Cellular & molecular immunology*. 2013;10:151-8.
45. Wan M, Li C, Zhen G, Jiao K, He W, Jia X. et al. Injury-activated transforming growth factor beta controls mobilization of mesenchymal stem cells for tissue remodeling. *Stem cells*. 2012;30:2498-511.
46. Julier Z, Park AJ, Briquez PS, Martino MM. Promoting Tissue Regeneration by Modulating the Immune System. *Acta Biomaterialia*. 2017;53.
47. Bank RA, Zandstra J, Room H, Petersen AH, van Putten SM. Biomaterial Encapsulation Is Enhanced in the Early Stages of the Foreign Body Reaction During Conditional Macrophage Depletion in Transgenic Macrophage Fas-Induced Apoptosis Mice. *Tissue Engineering Part A*. 2017;23.
48. Loi F, Cordova LA, Zhang R, Pajarinen J, Lin TH, Goodman SB. et al. The effects of immunomodulation by macrophage subsets on osteogenesis *in vitro*. *Stem Cell Research & Therapy*. 2016;7:15.
49. Dimitriou R, Tsiridis E, Giannoudis PV. Current concepts of molecular aspects of bone healing. *Injury*. 2005;36:1392-404.
50. Moore LB, Sawyer AJ, Saucier-Sawyer J, Saltzman WM, Kyriakides TR. Nanoparticle delivery of miR-223 to attenuate macrophage fusion. *Biomaterials*. 2016;89:127-35.
51. Kao WJ, McNally AK, Hiltner A, Anderson JM. Role for interleukin-4 in foreign-body giant cell formation on a poly (etherurethane urea) *in vivo*. *Journal of Biomedical Materials Research*. 1995;29:1267-75.
52. [Murray PJ, Wynn TA. Protective and pathogenic functions of macrophage subsets. *Nature reviews. Immunology*. 2011;11:723-37.
53. Sakurai E, Anand A, Ambati BK, van Rooijen N, Ambati J. Macrophage depletion inhibits experimental choroidal neovascularization. *Investigative ophthalmology & visual science*. 2003;44:3578-85.
54. Hibino N, Yi T, Duncan DR, Rathore A, Dean E, Naito Y. et al. A critical role for macrophages in neovessel formation and the development of stenosis in tissue-engineered vascular grafts. *FASEB journal : official publication of the Federation of American Societies for Experimental Biology*. 2011;25:4253-63.
55. Chen FM, Zhang M, Wu ZF. Toward delivery of multiple growth factors in tissue engineering. *Biomaterials*. 2010;31:6279-308.
56. Agarwal R, Garcia AJ. Biomaterial strategies for engineering implants for enhanced osseointegration and bone repair. *Advanced drug delivery reviews*. 2015;94:53-62.
57. Loi F, Cordova LA, Pajarinen J, Lin TH, Yao Z, Goodman SB. Inflammation, fracture and bone repair. *Bone*. 2016;86:119-30.
58. Shen X, Zhang Y, Gu Y, Xu Y, Liu Y, Li B. et al. Sequential and sustained release of SDF-1 and BMP-2 from silk fibroin-nanohydroxyapatite scaffold for the enhancement of bone regeneration. *Biomaterials*. 2016;106:205-16.
59. Horwood NJ. Macrophage Polarization and Bone Formation: A review. *Clinical reviews in allergy & immunology*. 2016;51:79-86.
60. Zhang Y, Bose T, Unger RE, Jansen JA, Kirkpatrick CJ, van den Beucken JJ. Macrophage type modulates osteogenic differentiation of adipose tissue MSCs. *Cell and tissue research*. 2017;369:273-86.
61. Geng Y, Zhang L, Fu B, Zhang J, Hong Q, Hu J. et al. Mesenchymal stem cells ameliorate rhabdomyolysis-induced acute kidney injury via the activation of M2 macrophages. *Stem Cell Research & Therapy*. 2014;5:1-14.
62. Luz-Crawford P, Jorgensen C, Djouad F. Mesenchymal Stem Cells Direct the Immunological Fate of Macrophages. Results and problems in cell differentiation. 2017;62:61-72.